Technometrics

ISSN: (Print) (Online) Journal homepage: https://www.tandfonline.com/loi/utch20

Statistical Modeling and Analysis of *k*-Layer Coverage of Two-Dimensional Materials in Inkjet Printing Processes

Jaesung Lee , Shiyu Zhou & Junhong Chen

To cite this article: Jaesung Lee , Shiyu Zhou & Junhong Chen (2020): Statistical Modeling and Analysis of *k*-Layer Coverage of Two-Dimensional Materials in Inkjet Printing Processes, Technometrics, DOI: 10.1080/00401706.2020.1805020

To link to this article: https://doi.org/10.1080/00401706.2020.1805020

TECHNOMETRICS
2020, VOL. 00, NO. 0, 1–11
https://doi.org/10.1080/00401706.2020.1805020

Taylor & Francis
Taylor & Francis Group

Statistical Modeling and Analysis of *k*-Layer Coverage of Two-Dimensional Materials in Inkjet Printing Processes

Jaesung Lee[a], Shiyu Zhou[a], and Junhong Chen[b,c]

[a]Department of Industrial and Systems Engineering, University of Wisconsin–Madison, Madison, WI; [b]Pritzker School of Molecular Engineering, University of Chicago, Chicago, IL; [c]Chemical Sciences and Engineering Division, Physical Sciences and Engineering Directorate, Argonne National Laboratory, Lemont, IL

ABSTRACT

Two-dimensional layered materials/flakes, also known as crystalline atom-thick layer nanosheets, have recently been receiving great attention in electronics fabrication due to their unique and intriguing properties. The *k*-layer coverage area (i.e., the area covered by *k* number of overlapping layers) of the printed flake pattern significantly impacts on the properties of the printed electronics. In this work, we constructed a statistical model to describe the *k*-layer coverage of randomly distributed two-dimensional materials. A series of results are obtained to provide not only the expectation but also the variance of the coverage area. The boundary effects on the random flakes coverage are also studied. In addition, an approximated statistical testing approach is also developed in this work to detect abnormal coverage patterns. The case studies based on simulated data and real flakes images obtained from the inkjet printing process demonstrate the accuracy and effectiveness of the proposed model and analysis methods.

ARTICLE HISTORY
Received June 2019
Accepted July 2020

KEYWORDS
Flake image; Inkjet printing process; Random coverage; Statistical quality control; Two-dimensional material

1. Introduction

Two-dimensional layered materials, also known as crystalline atom-thick layer nanosheets, have recently been receiving great attention in electronics fabrication due to their unique and intriguing properties. Graphene, for example, has high electronic and thermal conductivity, optical transparency, and mechanical strength and flexibility (Li, Lemme, and Östling 2014). After the discovery of an exfoliation method of graphene from graphite by Novoselov (2004), a large body of literature has been dealing with graphene and its variants, such as graphene oxide, as well as other two-dimensional materials, such as molybdenum disulfide (MoS_2). The inkjet printing technique has been gaining growing interests to fabricate electronics with these two-dimensional materials (Sowade et al. 2016). Inkjet printing is an additive patterning technique that deposits functional ink, which may contain two-dimensional m aterials as a solute, through nozzles onto the substrates. Inkjet-printed graphene and its variants have shown promising opportunities in a wide range of applications (Li et al. 2014), including sensors (Dua et al. 2010; Huang et al. 2011), wearable textiles (Li et al. 2012), antennas (Shin, Hong, and Jang 2011), and memory (Huber et al. 2017).

This article is motivated by the recently developed field-effect transistor (FET) sensors, which are used to detect the heavy metal ions in water (Chang et al. 2019). The sensor is illustrated in Figure 1. In such a sensor, the flakes of two-dimensional materials, namely rGO flakes, are inkjet-printed on the substrate. Two electrodes, named drain and source, are put on the printed pattern. As the gate voltage (denoted by V_g in the figure) is applied, the current between drain and source can be measured. When the sensor is exposed to the water contaminated by heavy metal ions, the current between the drain and source will deviate from its normal value.

The performance of the FET sensor is most significantly influenced by the coverage and thickness (i.e., number of overlapping layers) of flakes on the area between two electrodes. The FET sensor needs a high gap in the currents between on and off states. This can be achieved when flakes cover more surface with less flake overlap (Sui and Appenzeller 2009). In the inkjet printing process, flakes distribute randomly between the electrodes, and we cannot directly control them. It is highly desirable to have a model to describe and analyze the randomness in the coverage and the overlapping of randomly distributed two-dimensional materials. With such a model, we can link the process parameters to the flake distribution and predict the performance including both the sensitivity and repeatability of the fabricated sensors. In addition, we can use the model to identify if the flakes are uniformly distributed on the substrate, which is important for the process quality control purposes.

The existing literature on the random two-dimensional flakes coverage cannot address the practical needs in the inkjet-printing process. The study directly on the inkjet-printed pattern is mostly done based on the first principles. Researchers have investigated the drying process based on the physical movements of particles (Deegan et al. 1997; Fischer 2002; Hu and Larson 2006). The physics-based research gives insights into flakes behaviors during the ink's drying. However, the works in this category do not deal with the statistical behavior of

CONTACT Shiyu Zhou *szhou@engr.wisc.edu* Department of Industrial and Systems Engineering, University of Wisconsin–Madison, Madison, WI 53706.

Supplementary materials for this article are available online. Please go to *www.tandfonline.com/r/TECH*.

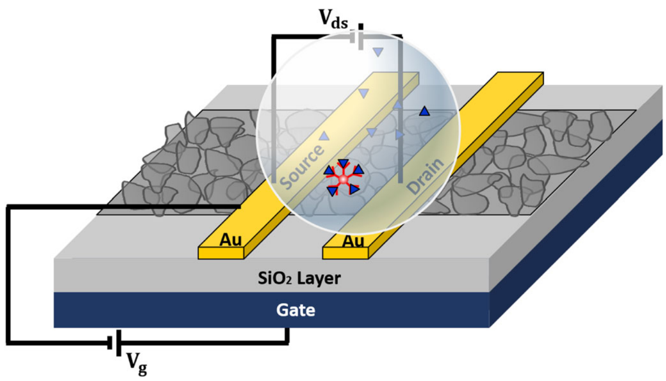

Figure 1. Field-effect transistor sensor for heavy metal detection in water.

flake coverage. The most widely known statistical model for the random two-dimensional coverage is the boolean model. The boolean model is based on the union set of every flake set whose location and shape is random (Chiu et al. 2013). The area covered by one or more layers is equally treated as *covered*, and the complement set as *uncovered*. The boolean model is popularly used in the literature on the coverage of random wireless sensor networks (Liu and Towsley 2003, 2004; Hsin and Liu 2004; Liu et al. 2005; Liu, Wu, and King 2005). There are two significant limitations of this model in pursuit of our objective. (1) It cannot explain multi-layer coverage. We need a more sophisticated model that can distinguish the thickness of the coverage because the performance of the electronics differs with respect to different thicknesses. (2) Its main focus is on the expectation of the coverage. To quantify the uncertainty in the manufacturing process, the variance of coverage should also be modeled and analyzed.

Some relevant literature can also be found in the application of randomly deployed wireless sensor networks. Their main interest is the detectability of special events such as wildfire by randomly deployed sensors. Many researchers have studied this field (Liu and Towsley 2003, 2004; Hsin and Liu 2004; Liu et al. 2005; Liu, Wu, and King 2005). However, it is hard to adopt these models because (1) fixed radius circular ranges are assumed, (2) only expectation is studied, (3) many works used the boolean model; therefore, they cannot distinguish different thicknesses. In Wan and Yi (2006), the authors studied the problem of a point/region being covered by *at least k* sensors. However, the *exact k*-layer coverage problem is not investigated. Furthermore, in their study, the coverage area of a single sensor is assumed to be a circle with a fixed radius. However, in the problem we are facing, flakes are randomly created from the ink fabrication process with different sizes and shapes. As a result, their model cannot address our needs.

In this article, to fill this research gap, we establish a statistical model that describes the uncertainties in the flakes dispersion and coverage with respect to different levels of thicknesses, namely *k-layer coverage fraction*, of the printed pattern. The flakes are defined by combining the uniformly distributed random locations and random shapes. A series of analytic results are obtained providing the expectation and variance of the coverage fraction with different thicknesses. The boundary effects on the random flakes coverage are also studied. Based on this model, we further propose a statistical testing method that detects the nonuniform printed pattern. These proposed models and methods are tested and validated through extensive numerical study and real flakes distribution images obtained from an inkjet process.

The rest of the article is organized as follows. Section 2 introduces the inkjet printing process and the relevant process parameters. Some basic assumptions on the flake distribution based on the process physics are also introduced. Section 3 delineates the proposed random flakes model and the expectation and variance of the coverage fraction with different thicknesses. The statistical testing approach to detect abnormal flake coverage is presented in Section 4. A numerical study that validates the proposed model is presented in Section 5. The validation based on the real flakes image is conducted in Section 6. Finally, we draw a conclusion and discussion in Section 7.

Table 1. Physical parameters.

Symbol	Definition
c_F	Mass concentration of the two-dimensional material flakes in the ink droplet
h_F	Height of the two-dimensional material flakes
ρ_F	Density of the two-dimensional material flakes
V_D	Volume of the ink droplet
θ_c	Contact angle of the ink droplet
R_F	Radius of the contact area of the ink droplet on the substrate

2. Inkjet Printing and Basic Assumptions

The inkjet printing process consists of two separate steps: ink preparation and inkjet printing. To provide the desired functionality, the ink is customized in the ink preparation step by controlling the mass concentration and size of the flakes in the ink (Figure 2(a)). First, two-dimensional material (e.g., graphene) flakes are exfoliated from crystal (e.g., graphite) and dissolved into the solvent up to the target mass concentration of the flakes in the ink. Then, the flakes sizes in the ink are reduced up to the target size by controlling the exposure time to the ultrasonic milling. The prepared ink is printed through the inkjet printer (Figure 2(b)). After the ink dries out, the dispersed flakes are left with a pattern, providing functionality. The real image of a flake pattern printed by an inkjet printer is presented in Figure 2(c) that is produced in He and Derby (2017).

The critical parameters in the printing step are summarized in Table 1. Among these parameters, h_F and ρ_F are constant material properties. The volume of the droplet ejected from an inkjet printer, V_D, can also be viewed as constant because V_D can be precisely controlled in a modern inkjet printing process (Singh et al. 2010) at picoliter level. Once the droplet falls on the substrate, it forms a spherical cap as shown in Figure 2(b). The contact angle θ_c is determined by the combination of the ambient temperature and the material properties of the substrate and droplet. The relationship among the droplet volume V_D, contact angle θ_c, and radius of the contact area R_F is given as (Picknett and Bexon 1977)

$$V_D = \frac{\pi}{3}(1-\cos\theta_c)^2(2+\cos\theta_c)\left(\frac{R_F}{\sin\theta_c}\right)^3. \tag{1}$$

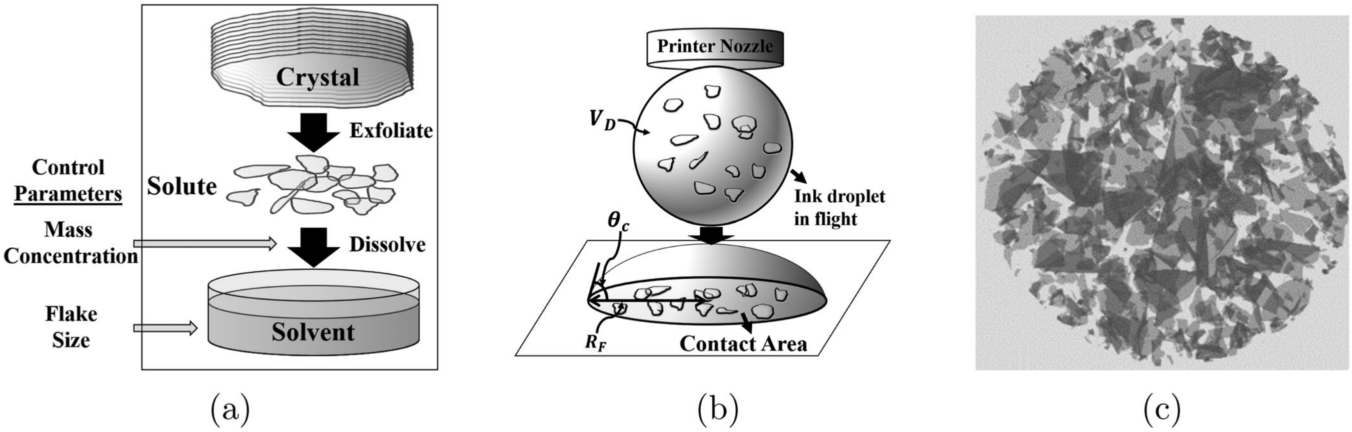

Figure 2. Two stages of two-dimensional material inkjet printing process are described: (a) ink preparation process and (b) inkjet printing process. (c) An image of the real pattern printed by an inkjet printer produced in He and Derby (2017).

R_F can be obtained given V_D and θ_c from (1). The mass concentration of the flakes in a droplet, c_F, is defined by the mass of the flakes in the ink droplet divided by the volume of the droplet. Due to the random dispersion of the flakes in the ink, c_F of different droplets are different. Thus, c_F of a droplet should be viewed as a random variable.

With $\mathbb{E}[c_F]$, we can derive the expected number of flakes in the droplet. Specifically, the mass of the flakes in the droplet is equal to the total summed sizes of flakes $\sum_{i=1}^{N} |F_i|$ multiplied by the height and density of the flakes, where $|F_i|$ denotes the area of ith flake and N is the number of flakes in the droplet; therefore, $\sum_{i=1}^{N} |F_i| = (c_F V_D) / (h_F \rho_F)$. Because the flake size $|F_i|$ is an independent random variable from each other and N, $\mathbb{E}_N \left[\mathbb{E} \left[\sum_{i=1}^{N} |F_i| \middle| N \right] \right] = \mathbb{E}_N \left[N \, \mathbb{E} \left[|F_i| | N \right] \right] = \mathbb{E}[N] \, \mathbb{E}[|F_i|]$. Then, the expectation of the number of flakes, $\mathbb{E}[N]$, is

$$\mathbb{E}[N] = \frac{\mathbb{E}[c_F] \, V_D}{\mathbb{E}[|F_i|] \, h_F \rho_F}. \tag{2}$$

According to the physical principles of the inkjet printing process, we can have the following three nonrestrictive assumptions:

- Flakes are uniformly distributed within the printed pattern: from a large body of literature, it is widely known that flakes are uniformly distributed when a coffee-ring does not form (Fischer 2002; He 2016).
- The number of flakes in a printed pattern is an independent Poisson random variable: the number of points drawn from an area where the point event occurrence follows the continuous uniform distribution is known to follow the Poisson distribution. This assumption has been widely used in the literature. For example, the number of printed cells in a printing process is known to follow the Poisson distribution (Merrin, Leibler, and Chuang 2007; Kim et al. 2016).
- Flake shape and size are independent random variables from the other process parameters: because the flake shape and size are determined before the printing process, the flake shapes and sizes are independent random variables from the other process parameters in the inkjet printing step.

The relationship in (2) and the above assumptions will be used in the following k-coverage model.

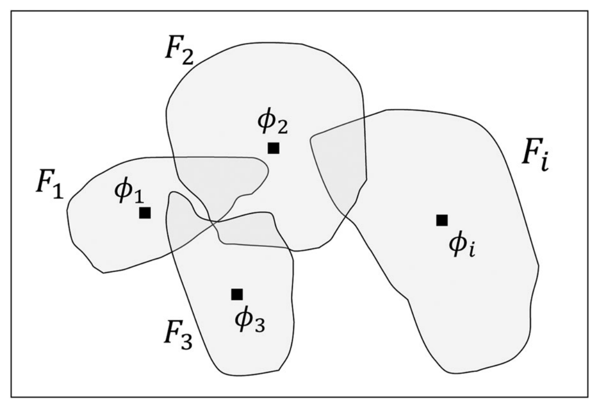

Figure 3. Random flakes are considered. The random flakes' center locations are uniformly distributed, and their shapes are defined by random compact sets.

3. *k*-Layer Random Coverage Fraction

3.1. Statistical Model of Flake Coverage

In this section, we propose a statistical flakes model that accounts for the random coverage and thickness of flakes in terms of the expectation and variance of the random coverage fraction. We consider random flakes. A flake F_i $(i = 1, \ldots, N)$ has its center location ϕ_i uniformly distributed over $\mathbb{S}_F \subset \mathbb{R}^2$, and $\mathbb{S}_F$ is the *flake space* or *printed space* within which flakes are deposited. The number of flakes N is a Poisson random variable with the parameter of mean $\mathbb{E}[N]$; thus, the flakes center locations $(\phi_1, \phi_2, \ldots)$ follow the Poisson process. The shape of the flake F_i is defined by an independent and identically distributed (iid) random compact set, and the size of the flake F_i is denoted by $|F_i|$. A rigorous definition of the random flakes is included in Appendix A.1 in the supplementary materials. The definition of the random flakes is illustrated in Figure 3.

Our objective is to study the expectation and variation of the coverage fraction that is covered by k layers of overlapping flakes, hereafter called k-layer coverage fraction, deposited in the space $\mathbb{S}_F$. The k-layer coverage fraction, denoted by $\mathcal{C}_k$, is evaluated by measuring the thickness at every point in $\mathbb{S}_F$ through the indicator $T_k(\mathbf{z})$ $(k = 0, 1, \ldots)$; $T_k(\mathbf{z})$ is a random variable that is 1 if the point $\mathbf{z} \in \mathbb{S}_F$ is covered by k layers of flakes or 0 otherwise. Conditioned on the point $\mathbf{z}$, $T_k(\mathbf{z})$ is a

Bernoulli random variable. $T_k(\mathbf{z})$ is statistically dependent on $T_k(\mathbf{w})$ for $\mathbf{w} \in \mathbb{S}_F$. Two points with a closer distance have a higher dependency because a near point $\mathbf{w}$ is also likely to be covered by the same flake covering $\mathbf{z}$. The k-layer coverage fraction, $\mathcal{C}_k$, can be calculated as

$$\mathcal{C}_k = \frac{\int_{\mathbf{z}\in\mathbb{S}_F} T_k(\mathbf{z})\, d\mathbf{z}}{\int_{\mathbf{z}\in\mathbb{S}_F} d\mathbf{z}}. \tag{3}$$

We first introduce the expectation and variance of $\mathcal{C}_k$ under the absence of the boundary effects in Sections 3.2.1 and 3.2.2. In general, the flake distribution close to the boundary of the printed area (i.e., the contact area of the droplet on the substrate) is different from the distribution around the center of the area. Such difference refers to the boundary effects. If the printed area is much larger than the size of flakes, the boundary effects can be ignored. Otherwise, the boundary effects may be significant. The boundary effects on the mean and variance of $\mathcal{C}_k$ are considered in Section 3.3. The method to calculate the exact expectation and variance with the random circular flakes is presented in Section 3.4. To make the flow smooth, the details of the mathematical derivations of these results are deferred to the supplementary materials.

3.2. k-Layer Coverage Fraction Without Boundary Effects

3.2.1. Expectation of k-Layer Coverage Fraction

The expectation of k-layer random coverage fraction is obtained by evaluating the thickness at every point over the space $\mathbb{S}_F$. The probability of any point $\mathbf{z}$ being covered by any k flakes is the same over $\mathbb{S}_F$ because every flake is uniformly distributed; therefore, $\mathbb{E}[\mathcal{C}_k] = \mathbb{E}[T_k(\mathbf{z})]$. Because $T_k(\mathbf{z})$ is a binary random variable, $\mathbb{E}[T_k(\mathbf{z})] = \mathbb{P}[T_k(\mathbf{z})]$ where $\mathbb{P}[T_k(\mathbf{z})]$ is the probability that a point $\mathbf{z}$ is covered by exact k flakes. Then, $\mathbb{E}[\mathcal{C}_k]$ is as follows.

$$\mathbb{E}[\mathcal{C}_k] = \mathbb{E}[T_k(\mathbf{z})] = \mathbb{P}[T_k(\mathbf{z})] = \frac{\exp\{-\mathbb{E}[N]p\}\left(\mathbb{E}[N]p\right)^k}{k!}, \tag{4}$$

where N is the number of flakes in $\mathbb{S}_F$ following the Poisson distribution, and p is the expected probability that a point $\mathbf{z}$ in $\mathbb{S}_F$ is covered by a single random flake:

$$p = \mathbb{E}\left[\frac{|F_i|}{|\mathbb{S}_F|}\right]. \tag{5}$$

We denote $p_i = |F_i|/|\mathbb{S}_F|$ as the probability that the flake F_i covers a point $\mathbf{z}$ (i.e., $p = \mathbb{E}[p_i]$). The result in (4) is obtained through deriving the probability that the point $\mathbf{z}$ is covered by any k among N flakes. The detailed derivation of (4) can be found in Appendix B.1 in the supplementary materials.

Point $\mathbf{z}$ is covered by the flake F_i when the flake's center location ϕ_i is located within a specific region, flip$(F_i, \mathbf{z}) \subset \mathbb{R}^2$; flip$(F_i, \mathbf{z})$ is defined as the region where F_i is rotated by 180° and translated so that its center is on $\mathbf{z}$ (Figure 4(a)). Because ϕ_i is uniformly distributed, the probability that ϕ_i is located within flip$(F_i, \mathbf{z})$ is $|F_i| / |\mathbb{S}_F|$, which does not rely on the flake center location ϕ_i nor the point $\mathbf{z}$. The rationale for using flip$(F_i, \mathbf{z})$ is illustrated in Figure 4(b). For the flake F_i to cover $\mathbf{z}$, the distance between ϕ_i and $\mathbf{z}$ must be shorter than the distance between ϕ_i and α that is the point where a line from ϕ_i crossing $\mathbf{z}$ meets the boundary of the flake. Equivalently, if ϕ_i falls in between α' and $\mathbf{z}$, meaning ϕ_i is within flip$(F_i, \mathbf{z})$, $\mathbf{z}$ is covered by the flake. The mathematical definition of flip$(F_i, \mathbf{z})$ can be found in Appendix A.2 of the supplementary materials.

The expectation of $\mathcal{C}_k$ is in the form of the Poisson probability mass function with its parameter $\mathbb{E}[N]\,p$. It is notable that $\mathbb{E}[\mathcal{C}_k]$ does not depend on the individual flake size or shape, but it is determined by $\mathbb{E}[N]\,p = \mathbb{E}\left[\sum_i^N |F_i|\right] / |\mathbb{S}_F|$, which is the relative total size of the flakes to the size of the printed pattern. This relative size is proportional to the mass concentration of the flakes in the ink. In other words, $\mathbb{E}[\mathcal{C}_k]$ is determined by the mass concentration.

3.2.2. Variance of k-Layer Coverage Fraction

The variance of $\mathcal{C}_k$ is obtained through the spatial correlation, which is represented by the covariance or the correlation coefficient, of the thickness at every pair of two points in $\mathbb{S}_F$.

$$\mathrm{var}[\mathcal{C}_k] = \frac{1}{|\mathbb{S}_F|^2}\left\{\int_{\mathbf{z}\in\mathbb{S}_F}\int_{\mathbf{w}\in\mathbb{S}_F} \mathrm{cov}[T_k(\mathbf{z}), T_k(\mathbf{w})]\, d\mathbf{w}\, d\mathbf{z}\right\}, \tag{6}$$

$$= \mathrm{var}[T_k(\mathbf{z})]\frac{\int_{\mathbf{z}\in\mathbb{S}_F}\int_{\mathbf{w}\in\mathbb{S}_F} \mathrm{corr}[T_k(\mathbf{z}), T_k(\mathbf{w})]\, d\mathbf{w}\, d\mathbf{z}}{|\mathbb{S}_F|^2}$$

$$\leq \mathrm{var}[T_k(\mathbf{z})], \tag{7}$$

where cov is covariance and corr is correlation coefficient. The detailed mathematical derivations of (6), (7), and the following results regarding the variance can be found in Appendix

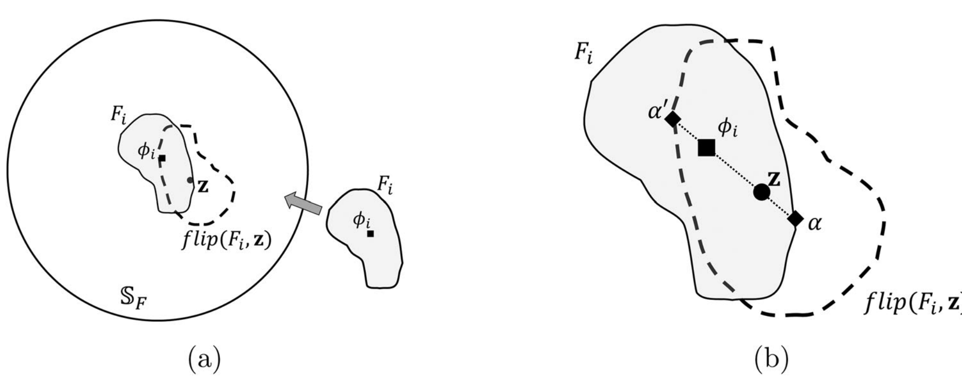

Figure 4. (a) The event that a point $\mathbf{z}$ is covered by the flake F_i is equivalent to the event that the center location ϕ_i is located within the dashed area, denoted by flip$(F_i, \mathbf{z})$ (point reflection of F_i whose center is on $\mathbf{z}$). (b) Illustration of rationale for using flip$(F_i, \mathbf{z})$.

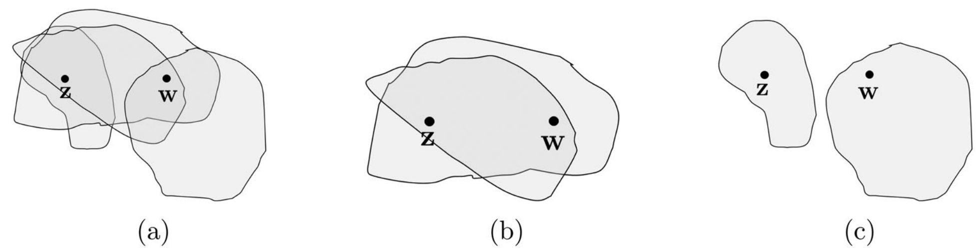

Figure 5. The event that two points are covered by k layers can be divided into $k+1$ mutually exclusive collectively exhaustive subevents: points $\mathbf{z}$ and $\mathbf{w}$ are covered by the same l flakes and by $k-l$ layers of different flakes. The subevent when $l=2, k=3$ is illustrated in (a). Two points are covered by l layers with the same flakes in (b) and by $k-l$ layers with different flakes in (c).

B.2 in the supplementary materials. $\text{var}\left[\mathcal{C}_k\right]$ can be decomposed into two parts, $\text{var}\left[T_k(\mathbf{z})\right]$ and the normalized integration of $\text{corr}\left[T_k(\mathbf{z}), T_k(\mathbf{w})\right]$. $\text{var}\left[T_k(\mathbf{z})\right]$ can be found in terms of $\mathbb{E}\left[T_k(\mathbf{z})\right]$ (presented in (4)): $\text{var}\left[T_k(\mathbf{z})\right] = \mathbb{E}\left[T_k(\mathbf{z})\right] - \mathbb{E}\left[T_k(\mathbf{z})\right]^2$, for any $\mathbf{z}$ in $\mathbb{S}_F$. Therefore, $\text{var}\left[T_k(\mathbf{z})\right]$ does not rely on the individual flake shapes or sizes but it relies on the total size of the flakes. In contrast, smaller flakes will produce smaller correlations of the thickness at two different points ($\text{corr}\left[T_k(\mathbf{z}), T_k(\mathbf{w})\right]$), leading to a smaller variance of $\mathcal{C}_k$. The upper-bound of $\text{var}\left[\mathcal{C}_k\right]$ is $\text{var}\left[T_k(\mathbf{z})\right]$ by setting $\text{corr}\left[T_k(\mathbf{z}), T_k(\mathbf{w})\right] = 1$ for all $\mathbf{z}$ and $\mathbf{w}$. However, this upper-bound is generally not tight.

We can also obtain a more detailed expression of $\text{cov}\left[T_k(\mathbf{z}), T_k(\mathbf{w})\right]$ as

$$\sum_{l=0}^{k} \frac{\mathbb{E}\left[N\right]^{2k-l} p_{\mathbb{I}}(\mathbf{z},\mathbf{w})^l \left\{p - p_{\mathbb{I}}(\mathbf{z},\mathbf{w})\right\}^{2(k-l)}}{l! \left\{(k-l)!\right\}^2} \times \exp\left\{-\mathbb{E}\left[N\right]\left(2p - p_{\mathbb{I}}(\mathbf{z},\mathbf{w})\right)\right\} - \mathbb{E}\left[\mathcal{C}_k\right]^2, \tag{8}$$

where $p_{\mathbb{I}}(\mathbf{z},\mathbf{w}) = \mathbb{E}\left[p_{\mathbb{I}i}(\mathbf{z},\mathbf{w})\right]$ is the expected probability that two points $\mathbf{z}$ and $\mathbf{w}$ are covered by a single random flake, and $p_{\mathbb{I}i}(\mathbf{z},\mathbf{w}) = \mathbb{P}\left[\mathbf{z} \in F_i \cap \mathbf{w} \in F_i\right]$ is the probability that the both points are covered by the same flake F_i, which can be written as

$$p_{\mathbb{I}i}(\mathbf{z},\mathbf{w}) = \frac{\left|\left(\text{flip}\left(F_i, \mathbf{z}\right)\right) \cap \left(\text{flip}\left(F_i, \mathbf{w}\right)\right)\right|}{\left|\mathbb{S}_F\right|}. \tag{9}$$

The basic idea to obtain (8) is that $\text{cov}\left[T_k(\mathbf{z}), T_k(\mathbf{w})\right]$ can be calculated with the probability of an event that two points $\mathbf{z}$ and $\mathbf{w}$ are both covered by k flakes ($\mathbb{P}\left[T_k(\mathbf{z}) = 1,\ T_k(\mathbf{w}) = 1\right]$). This event can be divided into $k+1$ mutually exclusive collectively exhaustive subevents: both points $\mathbf{z}$ and $\mathbf{w}$ are covered by the l same flakes ($l = 0, 1, \ldots, k$) and by $(k-l)$ layers with different flakes (Figure 5).

The covariance of two different levels of coverage fractions $\text{cov}\left[\mathcal{C}_k, \mathcal{C}_h\right]$ can be calculated in a similar manner.

$$\begin{aligned}
&\text{cov}\left[\mathcal{C}_k, \mathcal{C}_h\right] \\
&= \frac{1}{\left|\mathbb{S}_F\right|^2} \int_{\mathbf{z}}\int_{\mathbf{w}} \sum_{l=0}^{\min(k,h)} \frac{\mathbb{E}\left[N\right]^{k+h-l} p_{\mathbb{I}}(\mathbf{z},\mathbf{w})^l \left\{p - p_{\mathbb{I}}(\mathbf{z},\mathbf{w})\right\}^{(k+h-2l)}}{l! \left\{(k-l)!\right\}^2} \\
&\quad \times \exp\left[-\mathbb{E}\left[N\right]\left\{2p - p_{\mathbb{I}}(\mathbf{z},\mathbf{w})\right\}\right] - \mathbb{E}\left[\mathcal{C}_k\right]\mathbb{E}\left[\mathcal{C}_h\right] d\mathbf{w} d\mathbf{z},
\end{aligned} \tag{10}$$

where $\text{var}\left[\mathcal{C}_k\right] = \text{cov}\left[\mathcal{C}_k, \mathcal{C}_k\right]$.

Notice that $p_{\mathbb{I}i}(\mathbf{z},\mathbf{w})$ in (9) depends on the shape of the flakes. Consider, for example, two different shapes of flakes, circle and ellipse, that have the same size $|F_i|$. Then, because the sizes of the flakes are given the same, the major axis of the elliptical flake is longer than the diameter of the circular flake. Therefore, there will exist some points $\mathbf{z}$ and $\mathbf{w}$ that the circular flake cannot cover both points ($p_{\mathbb{I}i}(\mathbf{z},\mathbf{w}) = 0$) whereas the wider elliptical flake can cover the both points ($p_{\mathbb{I}i}(\mathbf{z},\mathbf{w}) > 0$).

In the following section, the expectation and variance of $\mathcal{C}_k$ with boundary effects are presented.

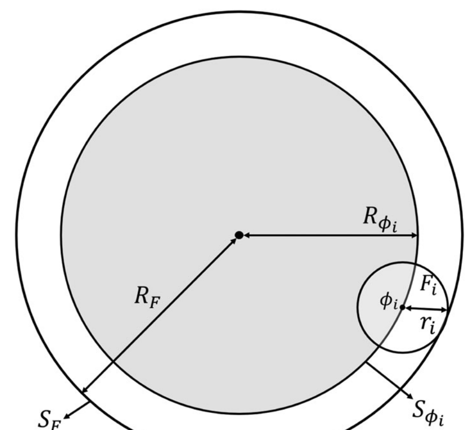

Figure 6. With the boundary condition, the center point space $\mathbb{S}_{\phi_i}$, where the center point of flake F_i can be located, depends on the size of the flake.

3.3. *k*-Layer Coverage Fraction Considering Boundary Effects

The boundary effects can be ignored when the size of the printed region $\mathbb{S}_F$ is significantly larger than the flakes sizes. However, the boundary effect may not be ignored when $\mathbb{S}_F$ is not large compared to the sizes of the flakes.

The boundary of the ink droplet restricts whole flakes to be located within it, which forces the flake center location ϕ_i to be placed in a smaller space $\mathbb{S}_{\phi_i} \subset \mathbb{S}_F$. The mathematical definition of $\mathbb{S}_{\phi_i}$ can be found in Appendix A.3 in the supplementary materials. This restriction causes complications in the calculation of the mean and variance of k-layer coverage fractions. This restricted flake center space is illustrated in Figure 6.

With the boundary effects, the mean and variance of k-layer coverage fraction presented in (4) and (10) still hold, but the parameter $p(\mathbf{z})$ and $p_{\mathbb{I}}(\mathbf{z},\mathbf{w})$ need to be adjusted accordingly. Although $p(\mathbf{z})$ is constant over the space $\mathbb{S}_F$ when the boundary effects are considered, $p(\mathbf{z})$ relies on point $\mathbf{z}$ with the consideration of boundary effects because of the restriction of $\mathbb{S}_{\phi_i}$. Now, flake F_i covers point $\mathbf{z}$ if the flake's center is located within $\mathbb{S}_{\phi_i} \cap (\text{flip}(F_i, \mathbf{z}))$ among its possible position $\mathbb{S}_{\phi_i}$. Thus, $p(\mathbf{z})$ is

$$p(\mathbf{z}) = \mathbb{E}\left[\frac{\left|\mathbb{S}_{\phi_i} \cap \left(\text{flip}(F_i, \mathbf{z})\right)\right|}{\left|\mathbb{S}_{\phi_i}\right|}\right]. \tag{11}$$

Similarly, $p_{I\!I}(\mathbf{z}, \mathbf{w})$ is as follows.

$$p_{I\!I}(\mathbf{z}, \mathbf{w}) = \mathbb{E}\left[\frac{\left|\mathbb{S}_{\phi_i} \cap \left(\text{flip}(F_i, \mathbf{z})\right) \cap \left(\text{flip}(F_i, \mathbf{w})\right)\right|}{\left|\mathbb{S}_{\phi_i}\right|}\right]. \tag{12}$$

3.4. k-Layer Coverage Fraction for Circular Flakes

3.4.1. k-Layer Coverage Fraction Without Boundary Effects

Calculation of $\text{var}[\mathcal{C}_k]$ involves $p_{I\!I}(\mathbf{z}, \mathbf{w})$, which relies on the shape of the flakes. In this section, we show how to calculate $p_{I\!I}(\mathbf{z}, \mathbf{w})$ based on the random sized circular flakes; the random radius is denoted by r_i, and its probability density function is denoted by $f(r_i)$. The robustness of the outcome with respect to different flake shapes are presented in the numerical study.

With circular flakes, now, $\left|\left(\text{flip}(F_i, \mathbf{z})\right) \cap \left(\text{flip}(F_i, \mathbf{w})\right)\right|$ in (9) reduces to $|\mathcal{D}(\mathbf{z}, r_i) \cap \mathcal{D}(\mathbf{w}, r_i)|$ where $\mathcal{D}(\mathbf{z}, r_i) = \{x \mid \|x - \mathbf{z}\| \leq r_i\}$ is a circular disc whose radius is r_i and center is on $\mathbf{z}$. Now, $|\mathcal{D}(\mathbf{z}, r_i) \cap \mathcal{D}(\mathbf{w}, r_i)|$ can be found in a closed form (shaded area in Figure 7). Therefore, $p = \mathbb{E}[p_i]$ and $p_{I\!I}(\mathbf{z}, \mathbf{w}) = \mathbb{E}\left[p_{I\!I\,i}(\mathbf{z}, \mathbf{w})\right]$ can be obtained as follows.

$$p = \frac{r^2}{R_F^2}, \tag{13}$$

$$p_{I\!I}(\mathbf{z}, \mathbf{w}) = \frac{1}{|\mathbb{S}_F|}\int_{r=\frac{d}{2}}^{\infty} f(r)\left\{2r^2\cos^{-1}\frac{d}{2r} - d\sqrt{r^2 - \frac{d^2}{4}}\right\} dr. \tag{14}$$

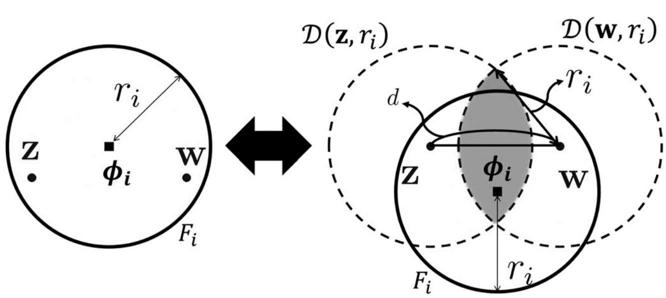

Figure 7. A circular flake covers both points **z** and **w** if and only if the center of the flake (square dot, ϕ_i) is located within the overlap of $\mathcal{D}(\mathbf{z}, r_i)$ and $\mathcal{D}(\mathbf{w}, r_i)$ (shaded area) where $\mathcal{D}(\mathbf{z}, r_i)$ is a circular disc whose center is **z** with radius r_i.

3.4.2. k-Layer Coverage Fraction With Boundary Effects

With the boundary effects, to calculate $p(\mathbf{z})$ and $p_{I\!I}(\mathbf{z}, \mathbf{w})$, a complex geometrical relationship needs to be considered: $\mathbb{S}_{\phi_i} \cap (\text{flip}(F_i, \mathbf{z}))$ and $\mathbb{S}_{\phi_i} \cap (\text{flip}(F_i, \mathbf{z})) \cap (\text{flip}(F_i, \mathbf{w}))$. To make the problem tractable, we propose an approximation method to estimate $p(\mathbf{z})$ and $p_{I\!I}(\mathbf{z}, \mathbf{w})$ by reducing the space to be evaluated.

We want to study $\mathbb{E}[\mathcal{C}_k]$ and $\text{var}[\mathcal{C}_k]$ over a reduced space $\mathbb{S}_e$, namely *evaluation space*. In particular, we want to precisely estimate $p(\mathbf{z})$ and $p_{I\!I}(\mathbf{z}, \mathbf{w})$ for $\mathbb{E}[\mathcal{C}_k]$ and $\text{var}[\mathcal{C}_k]$ while losing the least amount of information on the coverage. We specify $\mathbb{S}_e$ as follows.

$$\mathbb{S}_e = \{\mathbf{z} | \mathbb{P}(\|\mathbf{z}\| > R_F - 2r_i) \leq \varepsilon\}, \tag{15}$$

where ε is a very small number, and $\|\cdot\|$ is the Euclidean distance from the origin. We used 0.001 for ε for this work. Under $\mathbb{S}_e$, $p_i(\mathbf{z})$ is approximated as follows.

$$p_i(\mathbf{z}) \approx \tilde{p}_i = \frac{|F_i|}{\left|\mathbb{S}_{\phi_i}\right|}. \tag{16}$$

Figure 8 shows p_i values with respect to different $\|\mathbf{z}\|$. When $\mathbf{z}$ falls in $\|\mathbf{z}\| \leq R_{c_i} = R_F - 2r_i$, p_i is constant as $\tilde{p}_i$, and as $\|\mathbf{z}\|$ surpasses R_{c_i}, p_i diminishes to zero at R_F. Therefore, all the points $\mathbf{z} \in \mathbb{S}_e$, will be exactly evaluated by the true value $\tilde{p}_i$ with the probability of $1 - \varepsilon$ (Figure 8(a)). When the flake radius is very large, some points $\mathbf{z}$ where $R_{c_i} \leq \|\mathbf{z}\| \leq R_e$ have p_i smaller than $\tilde{p}_i$ with a small chance ε (Figure 8(b)). Therefore, $p(\mathbf{z})$ will be slightly overestimated. $p_{I\!I}(\mathbf{z}, \mathbf{w})$ is also calculated similarly.

Then, $p(\mathbf{z})$ and $p_{I\!I}(\mathbf{z}, \mathbf{w})$ can be obtained as follows.

$$p(\mathbf{z}) = \int_{r=0}^{R_F/2}\left\{\frac{r^2}{(R_F - r)^2}\right\} f(r)\, dr + \int_{R_F/2}^{\infty} f(r)\, dr, \tag{17}$$

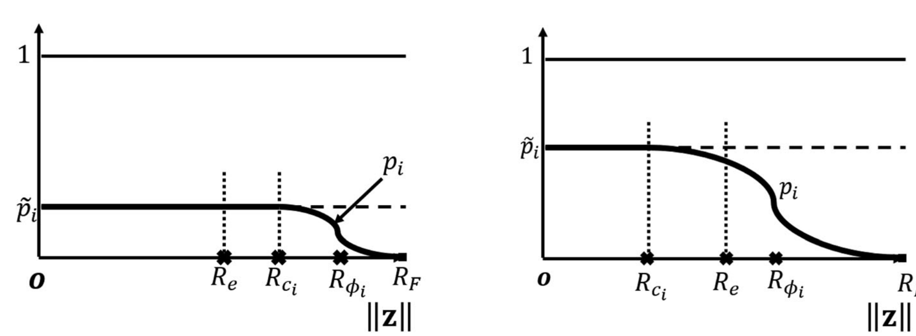

(a) p_i is constant within $\|\mathbf{z}\| < R_e$ when the flake radius is small and $r_i \leq 0.5(R_F - R_e)$

(b) p_i reduces within $\|\mathbf{z}\| < R_e$ as $\|\mathbf{z}\|$ increases when the flake radius is large and $r_i > 0.5(R_F - R_e)$

Figure 8. The probability that a point is covered by k layers of flakes is affected by the boundary effect.

$$p_{\mathbb{I}}(\mathbf{z},\mathbf{w}) = \int_{r=0}^{R_F/2} \left\{ \frac{|\mathcal{D}(\mathbf{z},r) \cap \mathcal{D}(\mathbf{w},r)|}{(R_F-r)^2} \right\} f(r)\, dr + \int_{R_F/2}^{\infty} f(r)\, dr, \tag{18}$$

where $\mathcal{D}(\mathbf{z},r)$ is a circular disc whose center is on $\mathbf{z}$ with radius r, and $|\mathcal{D}(\mathbf{z},r) \cap \mathcal{D}(\mathbf{w},r)| = 2r^2\cos^{-1}(d/2r) - d\sqrt{r^2 - d^2/4}$.

This method provides a quite accurate approximation of the k-coverage fractions with the boundary effects. Its accuracy is validated in the numerical studies.

4. Statistical Testing for Nonuniform Coverage Patterns

The expectation and variance of coverage fraction we have derived are based on the assumption that the flake center points $(\phi_1, \phi_2, \ldots)$ are uniformly distributed. Therefore, when the flakes are no longer distributed uniformly, the distribution of $\mathcal{C}_k$, along with $\mathbb{E}[\mathcal{C}_k]$ and $\mathrm{var}[\mathcal{C}_k]$, changes. Based on this property, we provide a statistical testing method to detect the nonuniform patterns based on the k-layer coverage fraction $\mathcal{C}_k$ evaluated from the real image. In the inkjet printing process, some combination of unfavorable process conditions may lead to a "coffee-ring" effect: most of the flakes will be clustered around the boundary of the printed region. Such an effect is very detrimental to the sensor performance, and we want to detect such a condition when it happens. Furthermore, due to the overlapping of flakes, it is generally very difficult to measure the center locations of the flakes from images. Thus, the flake center locations are not available to assess the flake distribution. Instead, $\mathcal{C}_k$ is generally obtainable from images. Therefore, the proposed method of testing the flake distribution based on $\mathcal{C}_k$ is very useful.

The hypothesis testing is based on the fact that $\mathcal{C}_k$ approximately follows the normal distribution. Billingsley (1995) showed that the summation of the associated Bernoulli random variables in a sequence follows the normal distribution asymptotically as the number of the random variables goes to infinity when the random variables far apart from each other in the sequence are nearly independent. This condition corresponds to the coverage fractions: $\mathcal{C}_k = \int_{\mathbf{z}\in\mathbb{S}_F} T_k(\mathbf{z}) / |\mathbb{S}_F|$ is the integration of the Bernoulli random variable $T_k(\mathbf{z})$ that has a nonzero correlation with $T_k(\mathbf{w})$ if $\mathbf{z}$ and $\mathbf{w}$ are close, but has a nearly zero correlation when $\mathbf{z}$ and $\mathbf{w}$ are distant due to the limitations in the flake sizes. In particular, as the correlation between two points lessens, the variances of the coverage fractions diminish, and the distribution of the coverage fractions gets closer to the normal distribution.

When the variance of $\mathcal{C}_k$ is large, however, its distribution may be discrepant from the normal. According to the previous analysis, we know larger flakes induce a larger variance of coverage fractions. Because flakes must be deposited through the inkjet printer nozzle, there exists a limitation in the size of printable flakes, relative to the size of the droplet. As a result, we can examine the distribution of the $\mathcal{C}_k$ in the worst-case scenario, when $\mathcal{C}_k$ has the largest variance. The largest printed flakes given nozzle sizes are investigated in He and Derby (2017). According to their study, we simulated flakes with $\mathbb{E}[r] = 17.95$, $\mathrm{Sd}[r] = 11.6$, $\mathbb{E}[N] = 122.1$, and $R_F = 180$ for the worst-case scenario with 1000 repetitions where Sd stands for the standard deviation. The histogram of the zero- and single-layer coverage fractions simulated based on the given parameters are Figure 9, and they are well fitted to the normal distribution. As the variances of the coverage fractions reduce, the coverage fractions fit better to the normal distribution.

With the normal approximation of the distribution of $\mathcal{C}_k$, a χ^2 test can be established. A vector of the multiple layer coverage fractions from zero- to (m-1)-overlapping flakes is defined by $\boldsymbol{\mathcal{C}}_m = (\mathcal{C}_0, \mathcal{C}_1, \ldots, \mathcal{C}_{m-1})^T$ with its mean $\mathbb{E}[\boldsymbol{\mathcal{C}}_m] = (\mathbb{E}[\mathcal{C}_0], \mathbb{E}[\mathcal{C}_1], \ldots, \mathbb{E}[\mathcal{C}_{m-1}])^T$, which are calculated through (4). The covariance matrix, $\Sigma_{\boldsymbol{\mathcal{C}}_m}$ where its kth diagonal component is $\mathrm{var}[\mathcal{C}_k]$ and its (k,h) element is $\mathrm{cov}[\mathcal{C}_k, \mathcal{C}_h]$, is calculated through (8) and (10). Then, the proposed statistic Q_m is as follows.

$$Q_m = (\boldsymbol{\mathcal{C}}_m - \mathbb{E}[\boldsymbol{\mathcal{C}}_m])^T \Sigma_{\boldsymbol{\mathcal{C}}_m}^{-1} (\boldsymbol{\mathcal{C}}_m - \mathbb{E}[\boldsymbol{\mathcal{C}}_m]) \sim \chi_m^2. \tag{19}$$

Q_m follows the chi-square distribution with the degree of freedom m. m can be selected based on how many layers are distinguishable in the image. Because many electronics require a low number of overlapping layers, m may not need to be large. We would like to mention that χ_m^2 distribution approximates Q_m very well. In the aforementioned worst-case, the false alarm probability of the test from the simulated data with 5000 iterations is 0.049 when we use $\chi_{1-0.05,m}^2$ as the critical value of the test. The actual false alarm probability is very close to the nominal value of 0.05.

The statistical testing can be performed as follows. First, $\mathbb{E}[\boldsymbol{\mathcal{C}}_m]$ and $\Sigma_{\boldsymbol{\mathcal{C}}_m}$ are calculated from (4), (8), and (10) with the printing parameters. Based on the image resolution, m, the number of distinguished layers from the image is determined. The upper control limit of the testing is set as $\chi_{1-\alpha,m}^2$ where $1-\alpha$ is the specified confidence level. Then, the coverage fractions $\mathcal{C}_k, k = 0, \ldots, m-1$, are measured from the printed pattern. When Q_m is larger than the upper control limit, the printed pattern is identified as nonuniform. Once Q_m is larger than the control limit, we know that the flakes are not uniformly distributed (with a probability of $1-(p\text{-value})$). This is because if the flakes were uniformly distributed, the mean and variance of

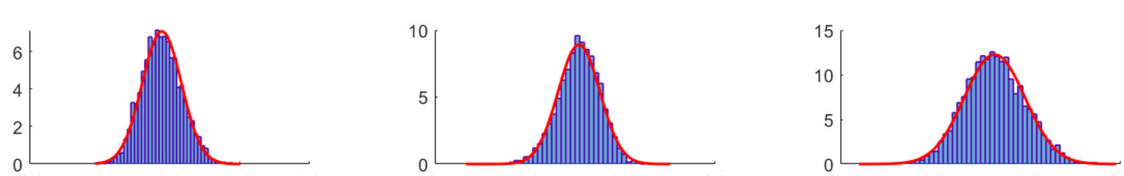

Figure 9. The histograms of $\mathcal{C}_0$ (left), $\mathcal{C}_1$ (center), and $\mathcal{C}_2$ (right) based on the simulated data suggest that they fit well to the normal distribution.

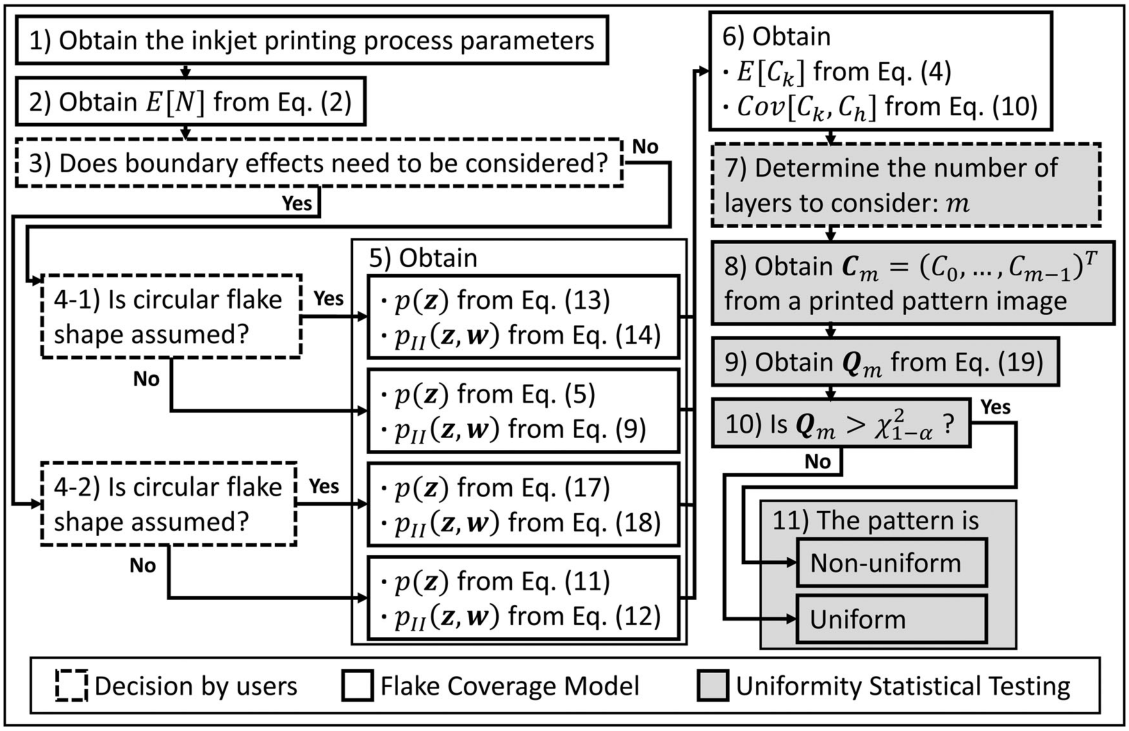

Figure 10. Summary of the implementation procedure.

Table 2. Summary of the parameters used in the numerical study.

Case	Parameter	Parameter values			Table index	
		Baseline	Setting 1(H)	Setting 2(L)	No boundary	Boundary
(i)	$E[\lvert F\rvert]$	98.17	392.70	3.93	Table A.3	Table A.8
	$Sd[\lvert F\rvert]$	117.87	471.47	4.71		
(ii)	$E[N]p$	1	1.5	0.5	Table A.4	Table A.9
(iii)	R_F	150	200	100	Table A.5	Table A.10
(iv)	Ratio(r)	0.5	0.7	0.3	Table A.6	Table A.11

the coverage fractions would be the same as the theoretical ones, and Q_m would not be significantly large under the chi-square distribution.

Figure 10 illustrates the implementation procedure to facilitate using the results in this work. In Figure 10, the decisions that users need to make are represented by the boxes with dashed-line boundaries, and the other processes are represented by the boxes with solid-line boundaries. The main outcome of our work consists of two parts: the mean and covariance of the flake coverage fractions and the uniformity statistical testing. The process of obtaining the outcomes of the flake coverage model is represented by the white boxes. The uniformity statistical testing process is represented in the gray boxes.

5. Numerical Study

In this section, the robustness of our proposed method is validated with different shapes of flakes (circle, ellipse, and rectangle) in various parameter settings. The parameter settings for the cases are shown in Table 2. For each case, we change one set of parameters (baseline case) to a higher level (Setting 1) or a lower level (Setting 2) while the other parameters are fixed.

Four parameters are selected to vary: (1) size of the flakes: mean and standard deviation of flake sizes ($\mathbb{E}[|F|]$ and $Sd[|F|]$) are varied. The baseline is where $\mathbb{E}[|F|] = 98.17$ and $Sd[|F|] = 117.87$ (which is when $\mathbb{E}[r] = 5$ and $Sd[r] = 2.5$ of circular flakes). They are changed into a high level ($\mathbb{E}[|F|] = 392.70$ and $Sd[|F|] = 471.47$ where $\mathbb{E}[r] = 10$ and $Sd[r] = 5$ of circular flakes) and a low level ($\mathbb{E}[|F|] = 3.93$ and $Sd[|F|] = 4.71$ where $\mathbb{E}[r] = 1$ and $Sd[r] = 0.5$ of circular flakes). (2) Flakes mass concentration: $E[N]p$, indicating the flakes mass concentration, is increased to 1.5 and reduced to 0.5. (3) Radius of the flake space: we considered a circular flake space with radius of $R_F = 150$, which is changed to 200 and 100. (4) Ratio of radius: the shapes of elliptical and rectangular flakes have varied. Ratio(r), the ratio between two axes of ellipse and rectangle (ratio between minor and major axes in an ellipse and ratio between width and length in a rectangle) is varied.

For each setting, we conducted the analysis both with and without the boundary effects. The outcomes from the simulation with three different flakes shapes (circle, ellipse, and rectangle) are presented along with the results calculated from the equations proposed in Section 3.4. The simulations are conducted with 1000 iterations. Because of the page limit, the detailed results are presented as tables in Appendix C in the supplementary materials. The table indexes can be found in

Table 2. From the numerical study results, we can observe the following characteristics:

1. The analytical results obtained in this article (based on Equations (4) and (8)) fit the simulation results very well. The expectations of the coverage fractions show little discrepancies among different shapes of flakes, and the outcomes based on our proposed equations are consistent with the simulated results. The flake shapes seldom affect the results. The standard deviations of the coverage fractions show larger differences than the expectations, but the discrepancies are still small. We can conclude that the expectation and standard deviation of the coverage fractions are robust to the flake shapes.
2. Without boundary effects, $\mathbb{E}[\mathcal{C}_0]$ and $\mathbb{E}[\mathcal{C}_1]$ are only determined by $E[N]p$. A larger mass concentration (indicated by large $E[N]p$) reduces the uncovered area. On the contrary, $\mathrm{Sd}[\mathcal{C}_0]$ and $\mathrm{Sd}[\mathcal{C}_1]$ are mainly affected by the relative size of the flakes to that of the printed pattern ($\mathbb{E}[|F_i|]$ / $|\mathbb{S}_F|$) as shown in Figure 11.
3. The impact of the boundary effects on $\mathcal{C}_0$ can be observed. $\mathbb{E}[\mathcal{C}_0]$'s are smaller when the boundary effects are considered in comparison to those without boundary effects. Especially, larger flakes show a large difference of $\mathbb{E}[\mathcal{C}_0]$. With the boundary effects, larger flakes tend to gather inside the flake space, leading to a reduction of $\mathbb{E}[\mathcal{C}_0]$. Inversely, a larger pattern size (larger radius of the printed pattern R_F) narrows the impacts of the boundary effects, meaning that a large printing area reduces the effects of the boundary. In general, as the flake sizes get smaller and as the size of the printed pattern R_F gets large, our proposed approximation method that considers the boundary effects becomes more accurate. Overall, $\mathbb{E}[\mathcal{C}_0]$ from the analytical equation (4) are smaller than those from the simulations. This is because we slightly overestimate the probability of a point being covered by a random flake.

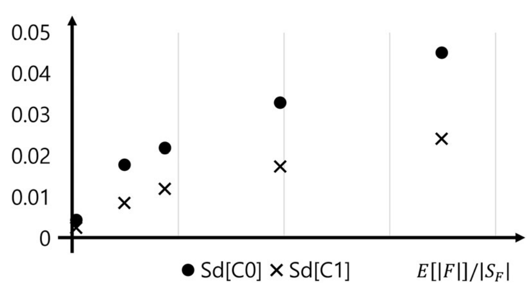

Figure 11. Changes in $\mathrm{Sd}\left[\mathcal{C}_k\right], k = 0, 1$.

6. Validation With Real Inkjet-Printed Flake Images

In this section, we show that the proposed model well describes the real flakes patterns produced by inkjet printing process, and the statistical testing scheme can detect nonuniform patterns. A flakes image is a surface topology image scanned by focused electron beams in the micrometer scale (also known as an SEM image). The original images are adopted from He and Derby (2017) and He (2016) with permission.

Six real images are presented in Figure 12. These are complete images of the dried droplets obtained from the inkjet printing processes. The physical parameters obtained from the printing process are summarized in Table 3 (He 2016). Figures 12(a)–(c)

Table 3. Physical parameters obtained from He (2016).

$\mathbb{E}[c_F]$	h_F	ρ_F	V_D	θ_C
0.5 mg/ml	1.0 nm	2200 mg/ml	0.77 nL	9.6 °

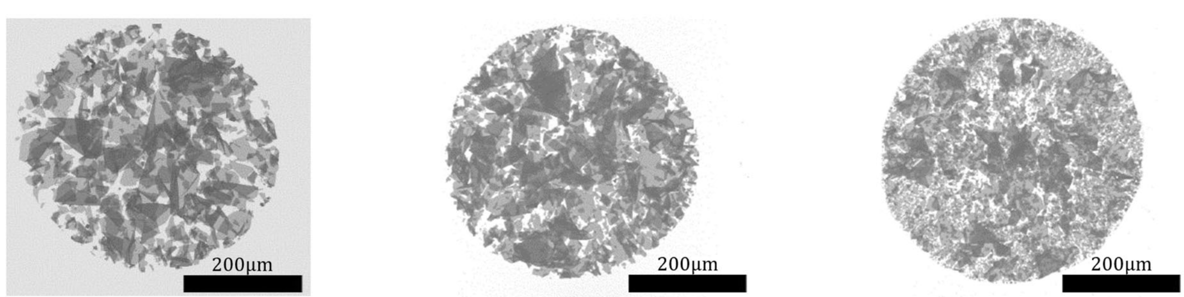

(a) $\mu_r = 17.95\mu m, \sigma_r = 11.6\mu m$ (b) $\mu_r = 10.85\mu m$, $\sigma_r = 7.9\mu m$ (c) $\mu_r = 3.55\mu m$, $\sigma_r = 4.5\mu m$

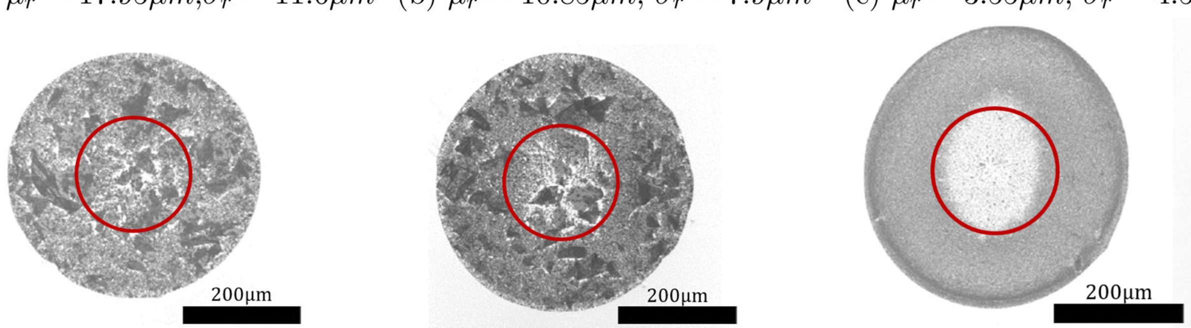

(d) $\mu_r = 1.85\mu m$, $\sigma_r = 1.9\mu m$ (e) $\mu_r = 0.9\mu m$, $\sigma_r = 2.15\mu m$ (f) $\mu_r = 0.475\mu m$, $\sigma_r = 0.225\mu m$

Figure 12. Real images of the patterns printed by inkjet printer.

show three uniform patterns, and Figures 12(d)–(f) show three nonuniform patterns that are widely known as the coffee-ring effect. When the coffee-ring appears, flakes are pushed forward and deposited near the boundary of the droplet; therefore, white blanks form in the center of the dried pattern. The coffee-rings in Figures 12(d) and (e) are quite subtle to observe without careful attention; thus, we marked the center of the images to highlight the coffee-ring effects. In Figures 12(d)–(f), large portions of white blanks are clearly observed in the center of the dried droplet. Additional information on these images is presented in Appendix D.1 in the supplementary materials.

To conduct the statistical testing, the zero- and single-layer coverage fractions, $\mathcal{C}_0$ and $\mathcal{C}_1$, are extracted from the real images as follows. First, the brightness values of the pixels inside the gray-scale image are plotted as a histogram (Figure 13). From the histogram, we can decide the cut-off brightness dividing each layer coverage. We used a heuristic method to determine the cut-off thresholds in this work, and the procedure is presented in Appendix D.2 in the supplementary materials. The proportions of zero- and single-layer coverage are obtained accordingly.

The extracted zero- and single-layer coverage fractions are presented in Table 4. In the table, $\mathbb{E}[r]$ and $\mathrm{Sd}[r]$ are the expectation and standard deviation of the radius of the flakes, which are provided in He and Derby (2017) and He (2016). The reduced space $\mathbb{S}_e$ is evaluated to deal with the boundary effects. $\mathcal{C}_0$ and $\mathcal{C}_1$ are the coverage fractions measured from the images. $\mathbb{E}[\mathcal{C}_k]$ and $\mathrm{Sd}[\mathcal{C}_k]$ are the expectation and standard deviation of the k-layer coverage fraction $\mathcal{C}_k$ calculated by Equations (4) and (8), and $\mathrm{cov}[\mathcal{C}_0, \mathcal{C}_1]$ is the covariance between $\mathcal{C}_0$ and $\mathcal{C}_1$ calculated by Equation (10). The chi-square statistics Q_2 calculated by Equation (19) are presented, followed by their p-values.

Based on the statistical testing, the images in Figures 12(a)–(c) are identified uniformly distributed with p-values larger than 0.1 while the images in Figures 12(d)–(f) are considered as nonuniform patterns with p-values less than 0.01. The case studies show that our proposed method can effectively catch the subtle nonuniformities of the pattern images.

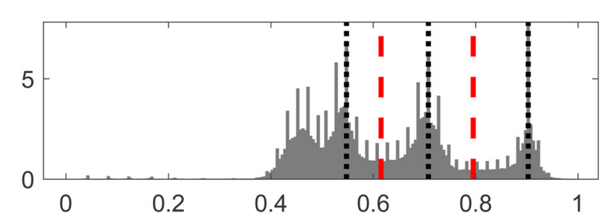

Figure 13. Histogram of the brightness of every pixel in the real inkjet-printed pattern image shown in Figure 12(a). Cut-off values for zero- and single-layer coverage are presented as vertical dashed lines.

The validation based on the real images suggests our proposed statistical model and the testing methods fit well with real data and can identify the nonuniform flakes dispersion pattern.

We would like to mention that the physical size of the images needs to be large enough to include a sufficient number of printed flakes. If an image is too small and includes only a limited number of flakes, the variance of the coverage fractions would be significantly large, and it will lead to a lower ability to identify the nonuniform patterns (i.e., a lower hypothesis testing power).

7. Conclusion

In this work, we constructed a statistical model to describe the k-layer coverage of randomly distributed two-dimensional materials. A series of results are obtained to provide not only the expectation but also the variance of coverage area. Compared with existing results, the proposed model considers the coverage with multiple overlapping layers and also provides the variance of the coverage area. To make our model more useful, boundary effects are also studied. With the boundary effects, a method to accurately evaluate the expectation and variance of k-layer coverage within a certain region is proposed. In addition, an approximated statistical testing approach is developed in this work to detect abnormal coverage patterns. The case studies based on the simulated data and real flake images obtained from the inkjet printing process show the accuracy and effectiveness of the proposed model and analysis methods. We expect the proposed model to be used to predict the functionality of the printed electronics and control the variability. The proposed statistical model may also be used in different applications. For example, our model can be used to describe the overlapping random coverage for the random wireless sensor network. Our proposed model can provide the prediction and quantification of variation where the detection ranges of the sensors are random.

We would like to mention that sometimes SEM image data might be expensive so that we may not be able to use these images for real-time quality control. However, even though the SEM image data are expensive, SEM images (or similar imaging data) are commonly available in modern microelectronic manufacturing processes, and these images can certainly be used for offline inspection and root cause analysis.

There are some interesting possible future directions. To calculate the variance of the coverage fractions in the integration, the circular shape of flakes was assumed in this work. However, if the flake shapes are far from circles, the result may not be sufficiently accurate. We can improve the accuracy of this model

Table 4. Case study outcome calculated by (4), (8), and (10) for the real images in Figure 12.

$\mathbb{E}[r]$	$\mathrm{Sd}[r]$	$\mathcal{C}_0$	$\mathcal{C}_1$	$\mathbb{E}[\mathcal{C}_0]$	$\mathbb{E}[\mathcal{C}_1]$	$\mathrm{Sd}[\mathcal{C}_0]$	$\mathrm{Sd}[\mathcal{C}_1]$	$\mathrm{cov}[\mathcal{C}_0, \mathcal{C}_1]$	Q_2	p-value
17.95	11.6	0.0977	0.2268	0.0773	0.1979	0.0542	0.0732	0.0028	0.18	0.9161
10.85	7.9	0.1039	0.2739	0.1041	0.2355	0.0414	0.0480	0.0015	1.39	0.499
3.55	4.5	0.1962	0.352	0.1081	0.2405	0.0460	0.0528	0.0021	4.49	0.1058
1.85	1.9	0.1451	0.353	0.1556	0.2895	0.0144	0.0122	0.0001	91.92	1.1×10^{-20}
0.9	2.15	0.125	0.659	0.1002	0.2305	0.0590	0.0712	0.0037	152.52	7.6×10^{-34}
0.475	0.225	0.217	0.5922	0.1768	0.3063	0.0010	0.0008	0	132,603	0

NOTE: For each printed pattern, statistical proportion test is conducted.

by using the observed flake shapes from the flake images directly onto the flake size and $p_{\mathbb{I}}(\mathbf{z}, \mathbf{w})$ estimations. For a more accurate estimate of the expected flake size, practitioners may use the flake images of patterns printed with diluted inks so that every flake is distinct and store the set of shapes of the flakes. Then, the mean flake size can be estimated based on the exact shape of the flakes, and accurate $p_{\mathbb{I}}(\mathbf{z}, \mathbf{w})$ may be estimated based on the observed shapes of flakes. Another possible direction of studying $p_{\mathbb{I}}(\mathbf{z}, \mathbf{w})$ would be the field of stochastic geometry, which has studied many aspects of the random geometry behaviors, including the boolean model. We plan to study these issues and report them in the future.

Supplementary Materials

Appendix: The mathematical details are included in Appendices A–D.
Matlab code: The matlab code for calculating the expectation and variance based on the analytical results presented in this work.

Funding

This work was supported by the National Science Foundation under grant number 1727846.

References

Billingsley, P. (1995), *Probability and Measure*, New York: Wiley. [7]

Chang, J., Pu, H., Wells, S. A., Shi, K., Guo, X., Zhou, G., Sui, X., Ren, R., Mao, S., Chen, Y., Hersam, M. C., and Chen, J. (2019), "Semi-Quantitative Design of Black Phosphorous Field-Effect Transistor Sensors for Heavy Metal Ion Detection in Aqueous Media," *Molecular Systems Design & Engineering*, 4, 491–502. [1]

Chiu, S. N., Stoyan, D., Kendall, W. S., and Mecke, J. (2013), *Stochastic Geometry and Its Applications*, New York: Wiley. [2]

Deegan, R. D., Bakajin, O., Dupont, T. F., Huber, G., Nagel, S. R., and Witten, T. A. (1997), "Capillary Flow as the Cause of Ring Stains From Dried Liquid Drops," *Nature*, 389, 827–829. [1]

Dua, V., Surwade, S., Ammu, S., Agnihotra, S., Jain, S., Roberts, K., Park, S., Ruoff, R., and Manohar, S. (2010), "All-Organic Vapor Sensor Using Inkjet-Printed Reduced Graphene Oxide," *Angewandte Chemie International Edition*, 49, 2154–2157. [1]

Fischer, B. J. (2002), "Particle Convection in an Evaporating Colloidal Droplet," *Langmuir*, 18, 60–67. [1,3]

He, P. (2016), "Inkjet Printing of Two Dimensional Materials," Ph.D. thesis, University of Manchester. [3,9,10]

He, P., and Derby, B. (2017), "Inkjet Printing Ultra-Large Graphene Oxide Flakes," *2D Materials*, 4, 021021. [2,3,7,9,10]

Hsin, C., and Liu, M. (2004), "Network Coverage Using Low Duty-Cycled Sensors," in *Proceedings of the Third International Symposium on Information Processing in Sensor Networks—IPSN'04*, ACM Press. [2]

Hu, H., and Larson, R. G. (2006), "Marangoni Effect Reverses Coffee-Ring Depositions," *The Journal of Physical Chemistry B*, 110, 7090–7094. [1]

Huang, L., Huang, Y., Liang, J., Wan, X., and Chen, Y. (2011), "Graphene-Based Conducting Inks for Direct Inkjet Printing of Flexible Conductive Patterns and Their Applications in Electric Circuits and Chemical Sensors," *Nano Research*, 4, 675–684. [1]

Huber, B., Popp, P. B., Kaiser, M., Ruediger, A., and Schindler, C. (2017), "Fully Inkjet Printed Flexible Resistive Memory," *Applied Physics Letters*, 110, 143503. [1]

Kim, Y. K., Park, J. A., Yoon, W. H., Kim, J., and Jung, S. (2016), "Drop-on-Demand Inkjet-Based Cell Printing With 30-μm Nozzle Diameter for Cell-Level Accuracy," *Biomicrofluidics*, 10, 064110. [3]

Li, J., Lemme, M. C., and Östling, M. (2014), "Inkjet Printing of 2D Layered Materials," *ChemPhysChem*, 15, 3427–3434. [1]

Li, J., Naiini, M. M., Vaziri, S., Lemme, M. C., and Östling, M. (2014), "Inkjet Printing of MoS_2," *Advanced Functional Materials*, 24, 6524–6531. [1]

Li, Y., Torah, R., Beeby, S., and Tudor, J. (2012), "An All-Inkjet Printed Flexible Capacitor on a Textile Using a New Poly(4-Vinylphenol) Dielectric Ink for Wearable Applications," in *2012 IEEE Sensors*, IEEE. [1]

Liu, B., Brass, P., Dousse, O., Nain, P., and Towsley, D. (2005), "Mobility Improves Coverage of Sensor Networks," in *Proceedings of the 6th ACM International Symposium on Mobile Ad Hoc Networking and Computing—MobiHoc'05*, ACM Press. [2]

Liu, B., and Towsley, D. (2003), "On the Coverage and Detectability of Large-Scale Wireless Sensor Networks," in *WiOpt'03: Modeling and Optimization in Mobile, Ad Hoc and Wireless Networks*, Sophia Antipolis, France. [2]

——— (2004), "A Study of the Coverage of Large-Scale Sensor Networks," in *2004 IEEE International Conference on Mobile Ad-Hoc and Sensor Systems (IEEE Cat. No.04EX975)*, IEEE. [2]

Liu, C., Wu, K., and King, V. (2005), "Randomized Coverage-Preserving Scheduling Schemes for Wireless Sensor Networks," in *NETWORKING 2005. Networking Technologies, Services, and Protocols; Performance of Computer and Communication Networks; Mobile and Wireless Communications Systems*, Springer Berlin Heidelberg, pp. 956–967. [2]

Merrin, J., Leibler, S., and Chuang, J. S. (2007), "Printing Multistrain Bacterial Patterns With a Piezoelectric Inkjet Printer," *PLoS ONE*, 2, e663. [3]

Novoselov, K. S. (2004), "Electric Field Effect in Atomically Thin Carbon Films," *Science*, 306, 666–669. [1]

Picknett, R., and Bexon, R. (1977), "The Evaporation of Sessile or Pendant Drops in Still Air," *Journal of Colloid and Interface Science*, 61, 336–350. [2]

Shin, K.-Y., Hong, J.-Y., and Jang, J. (2011), "Micropatterning of Graphene Sheets by Inkjet Printing and Its Wideband Dipole-Antenna Application," *Advanced Materials*, 23, 2113–2118. [1]

Singh, M., Haverinen, H. M., Dhagat, P., and Jabbour, G. E. (2010), "Inkjet Printing-Process and Its Applications," *Advanced Materials*, 22, 673–685. [2]

Sowade, E., Ramon, E., Mitra, K. Y., Martínez-Domingo, C., Pedró, M., Pallarès, J., Loffredo, F., Villani, F., Gomes, H. L., Terés, L., and Baumann, R. R. (2016), "All-Inkjet-Printed Thin-Film Transistors: Manufacturing Process Reliability by Root Cause Analysis," *Scientific Reports*, 6, 33490. [1]

Sui, Y., and Appenzeller, J. (2009), "Screening and Interlayer Coupling in Multilayer Graphene Field-Effect Transistors," *Nano Letters*, 9, 2973–2977. [1]

Wan, P.-J., and Yi, C.-W. (2006), "Coverage by Randomly Deployed Wireless Sensor Networks," *IEEE Transactions on Information Theory*, 52, 2658–2669. [2]